Non-linear modeling of the Edge Localized Modes and their control by Resonant Magnetic Perturbations in ASDEX Upgrade

F.Orain,[1] A.Lessig,[1] M.Hölzl,[1] E.Viezzer,[1] M.Dunne,[1] M.Bécoulet,[2] P.Cahyna,[3] G.T.A.Huijsmans,[2] M.Willensdorfer,[1] W.Suttrop,[1] A.Kirk,[4] S.Pamela,[4] S.Günter,[1] K.Lackner,[1] E.Strumberger,[1] D.Taray,[1] the ASDEX Upgrade Team,[1] and the EUROfusion MST1 Team*

(* see http://www.euro-fusionscipub.org/mst1)

[1]Max-Planck-Institut für Plasmaphysik, Garching, Germany

[2]CEA, IRFM, 13108 Saint-Paul-Lez-Durance, France

[3]IPP.CR, Prague, Czech Republic

[4]CCFE, Culham Science Centre, OX14 3DB, UK

Introduction: The experimental and theoretical study of Edge Localized Modes (ELMs) – occurring in the High confinement regime (H-mode) at the edge of tokamak plasmas – and their possible control methods (to mitigate the heat flux on divertor targets) is a crucial subject for current and future tokamaks. One foreseen ELM control method in ITER is the application of Resonant Magnetic Perturbations (RMPs), already proven capable to mitigate or suppress ELMs in existing tokamaks [1]. However significant progress in understanding the ELM dynamics, the plasma response to RMPs and the ELM interaction with RMPs is needed to improve predictive capabilities.

In this perspective, the ELM dynamics as well as the interaction between plasma and RMPs were modeled with the non-linear resistive MHD code JOREK with two-fluid effects [2,3]. The reconstructed ASDEX Upgrade equilibria and plasma parameters from H-mode discharges #23221 and #31128 [4] were used as input. A simulation is run as follows: first, the axisymmetric equilibrium is computed using temperature, density, current and toroidal rotation profiles. Two-fluid diamagnetic rotation (as well as neoclassical friction in the RMP section) are also included, impacting axisymmetric flows. Then $n \neq 0$ toroidal modes are included, allowing ELMs to grow, with or without the presence of RMPs. The dynamics of a "natural" ELM (without RMPs) is first considered and compared to experimental observations. In a second step, the plasma response to RMPs (without ELMs) is simulated.

ELM dynamics: A simplified picture of the ELM dynamics as observed in modeling (here using data from shot #23221) can be drawn as follows: the initially peeling-ballooning- (PB-)unstable profiles trigger the linear growth of the ELM (usually dominated in the linear phase by the most unstable mode), until the non-linear coupling between toroidal modes becomes important [5]. In this non-linear phase, density filamentary structures (Fig.1a) grow in the pedestal and are expelled across the separatrix, while energy is conducted towards the divertor targets, resulting in a collapse of the pressure profile. In this paper, we focus on two main aspects to compare with experimental observations: dominant mode numbers in the different phases of the ELM and dynamics of the filaments.

As previously noted in Ref.[6], for an accurate modeling of dominant mode numbers, it is important

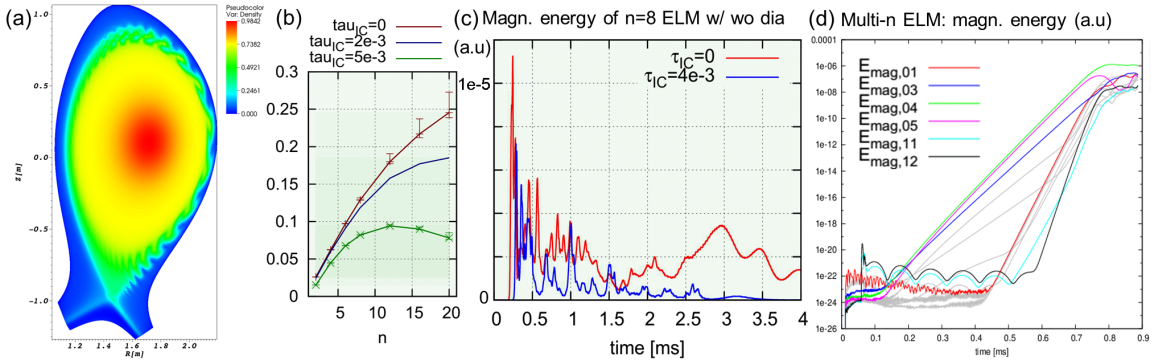

FIG. 1: (a) Poloidal section of the density during an ELM crash (normalized to central density). (b) Linear growth rate of modes depending on diamagnetic rotation: $\mathbf{V^*} = (\tau_{IC}/\rho)\ \mathbf{B} \times \nabla P$, where τ_{IC}, ρ and P are normalized ion cyclotron time, mass density and pressure. (c) Magnetic energy of the $n = 8$ mode with and without diamagnetic drifts. (d) Magnetic energy of n modes in multi-harmonic simulation of shot #31128.

to take into account the two-fluid diamagnetic rotation, as illustrated in Fig.1(b-c). In Fig.1b, the linear growth rate of the toroidal modes n is plotted without and with diamagnetic rotation in the model for two different diamagnetic velocities (the realistic one being for "tauIC=5e-3"). Without diamagnetic rotation, the most linearly-unstable mode is always the highest mode number, while with diamagnetic effects, the most unstable one lies between $n = 4$ and $n = 12$ ($n = 12$ in this case). This range matches experimental measurements of the mode numbers prior to the ELM crashes, using the magnetic pick-up coils [7]. The magnetic energy of an $n = 8$ ELM (in single harmonic simulations) is plotted with and without diamagnetic rotation in Fig.1c, where each energy spike corresponds to the expelling of a filament. Without diamagnetic drift, the energy of the mode is not damped after the ELM crash, and a state of "ballooning turbulence" keeps the plasma under the PB stability limit, preventing a second ELM crash to occur. However, when diamagnetic effects are included, they are capable to stabilise the plasma and allow to model the cyclic dynamics of ELMs [6].

In other recent modeling of the ELM dynamics for the shot #31128 (multi-harmonic $n = 1 - 12$ simulation, Fig.1d), the non-linear saturation of edge instabilities (after linear growth) is observed, inducing the saturation of the maximum pressure gradient, interestingly similar to experimental findings of [7]. The non-linear coupling between mid-range modes ($4 \leq n \leq 12$) in this saturated regime progressively leads to a dominant low n spectrum (here mainly $n = 1$). This observation, as well as the non-linear drive of $n = 1$ structures in the non-linear phase of the ELMs previously reported in [5], may fit with experimental observations in [7,8], where low n modes are the only remaining structures after the crash. Ongoing work aims at investigating in more detail the triggering of the main crash after the non-linear saturation and at closer comparisons to experiments.

As for the filament dynamics, an ELM (modeled for shot #23221) is characterized by the expulsion of several filaments. For each filament, the growth of finger-like structures of density (plotted at the outboard midplane in Fig.2c for different time steps of the ELM indicated in Fig.2a) is observed inside

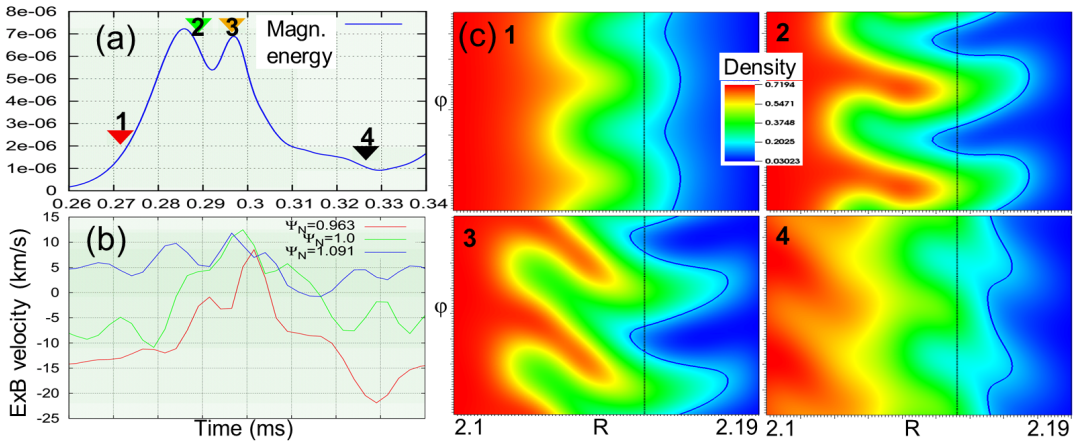

FIG. 2: (a) Magnetic energy of the $n = 8$ mode. (b) $E \times B$ velocity inside pedestal (red), on separatrix (green) and in the SOL (blue). (c) Density filaments for the times given in (a).

the pedestal, until they are large enough to cross the separatrix. The shear of the $E \times B$ velocity, as described in [9], generate the shearing and expelling of the filaments into the Scrape-Off-Layer (SOL). The time evolution of the $E \times B$ velocity at the outboard midplane inside the pedestal, at the separatrix and in the SOL, plotted in Fig.2b, show that filaments rotate in the pedestal in the $E \times B$ or electron diamagnetic direction, and are expelled in the SOL in the ion diamagnetic direction, in qualitative agreement with the Electron Cyclotron Emission Imaging (ECEI) measurement described in [10]. A more quantitative comparison will be the focus of future work.

Plasma response to RMPs: The plasma response to $n = 2$ RMPs (without ELMs, *i.e.* simulating only $n = 0$ and 2) is modeled using an equilibrium of shot #31128 for different applied RMP spectra. The spectrum is modified in experiment by changing the differential phase $\Delta\Phi$ between lower and upper RMP coils. Similarly to shot #30826 [4], $\Delta\Phi$ is scanned from $+90°$ to $-90°$ in the modeling. Experimentally, the strongest ELM mitigation is obtained for $+90°$, then the mitigated ELM frequency is reduced with $\Delta\Phi$ until $\Delta\Phi = -30°$, and an ELM-free phase is obtained between -30 and $-90°$. In modeling, even though RMPs are screened in the pedestal in all cases due to large electron perpendicular flows, the $\Delta\Phi = +90°$ case corresponds to the configuration for which the resonant response is strongest at the very edge, such that a larger ergodic layer is formed for normalized flux $\psi_{norm} > 0.97$ (Fig.3a), as compared to the $-90°$ case (Fig.3d). The Poincaré plots (Fig.3(a,d)) also show a larger kinking of field lines near the X-point for the $+90°$ case. This is due to the amplification of a stable edge kink modes $m > n \cdot q$ by magnetic perturbation, as observed in the 2D-Fourier spectrum of the magnetic flux perturbation, plotted in Fig.3b, where $m > n \cdot q$ harmonics are excited at the edge, contrary to the $-90°$ case (Fig.3e). It is actually this edge kink amplification that generates *via* poloidal coupling the maximum resonant response in the $+90°$ case, inducing a larger ergodic layer as well as larger lobe structures near the X-point. As seen in Fig.3(c), this strongest response also induces the largest 3D-displacement near the X-point, as compared to minimal displacement for

$\Delta\Phi = -90°$(Fig.3f).

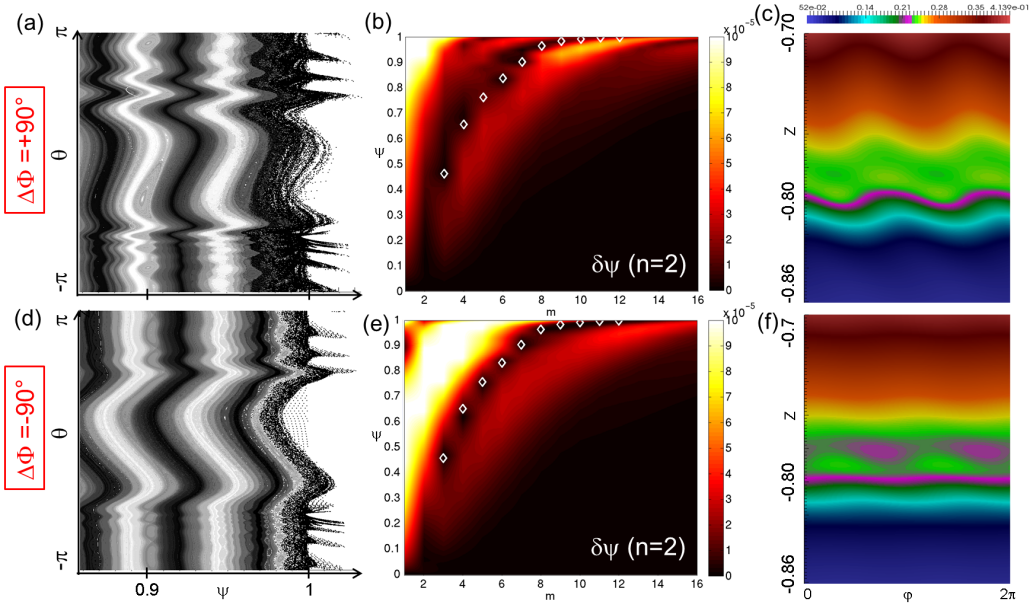

FIG. 3: (a,d) Poincaré plots of the magnetic topology at the plasma edge for coil configurations $\Delta\Phi = \pm 90°$. (b,e) ($n = 2$) perturbation of the magnetic flux as a function of the poloidal mode number m and the radial direction ψ_{norm}. Resonant surfaces are marked with white diamonds. (c,f) Vertical profile of the mass density around the X-point as a function of the toroidal angle φ.

Last, due to the plasma response to RMPs, the density pumpout ($\sim 10\%$ of density loss) observed in modeling is large enough to be highlighted, however not as large as in the experiment (up to $\sim 35\%$). More details about this work are provided in [11].

Conclusion: The modeling of the ELM dynamics in AUG with JOREK develops features such as mode number and filament dynamics qualitatively comparable to experiments. The study of the plasma response to RMPs in AUG shows that the strongest ELM mitigation in experiments is correlated with the strongest excitation of both the resonant response and the edge kink response coupled together. Current and future work aim at improving the picture of the ELM dynamics via simulations of several ELM cycles including a self-consistent bootstrap current model, with a more quantitative comparison to experiments. On the RMP side, future work will focus on a more accurate modeling of the density pumpout, and simulations of the interaction between ELMs and RMPs have been started, aiming to improve the understanding of ELM mitigation and suppression by RMPs.

References: [1] Y.Liang. Edge Localized Mode (ELM). In *Active Control of Magneto-Hydrodynamic Instabilities in Hot Plasmas*, Springer, 2015. [2] G.Huysmans and O.Czarny, *J. Comp. Phys.*, 227(16):7423-7445, 2008. [3] F.Orain *et al*, *Phys. Plas.*, 19(5):056105, 2013 [4] W.Suttrop *et al*, invited paper EPS 2016, submitted to *PPCF*. [5] I.Krebs *et al*, *Phys. Plas.* 20:082506, 2013. [6] Orain *et al*, *Phys. Rev. Letters*, 114 (3), 035001, 2015. [7] F.Mink *et al*, submitted to *PPCF*, 2016 [8] F.Laggner *et al*, *Plas. Phys. Contr. Fus.* 58:065005, 2016. [9] J.Morales *et al*, *Phys. Plas.* 23:042513, 2016. [10] Vanovac *et al*, this conference, P1.014. [11] F.Orain *et al*, *Nuc. Fus.* accepted, 2016.

Acknowledgement: *This work has been carried out within the framework of the EUROfusion Consortium and has received funding from the Euratom research and training programme 2014-2018 under grant agreement No 633053. The views and opinions expressed herein do not necessarily reflect those of the European Commission.*